Hindawi
Complexity
Volume 2019, Article ID 5834741, 14 pages
https://doi.org/10.1155/2019/5834741

*Research Article*

# Boost Converters' Proximate Constrained Time-Optimal Sliding Mode Control Based on Hybrid Switching Model

**Asghar Taheri**,[1,2] **Amir Ghasemian**,[2] **and Hai-Peng Ren**[1]

[1]*Xi'an Technological University, Xian 710021, China*
[2]*University of Zanjan, Zanjan 4537138791, Iran*

Correspondence should be addressed to Hai-Peng Ren; renhaipeng@xaut.edu.cn

Received 21 June 2019; Revised 19 August 2019; Accepted 28 August 2019; Published 27 October 2019

Guest Editor: Chun Wei



It is well known in the literature studies that the theoretical time-optimal control of boost converters can be achieved using switching surfaces based on the converter's natural state trajectories. However, this method has two important drawbacks: First, the transient current peak of the time-optimal controller is far beyond the current limitations of related circuit elements in many practical cases. Second, switching based on the converter's natural trajectories has high computational complexity and high dependence on circuit parameters. In this paper, based on the hybrid dynamical model of the converter and geometrical representation of its corresponding vector fields, a proximate constrained time-optimal sliding mode controller is proposed. The proposed method has a fast response that is near that of a time-optimal controller, with less computational complexity and sensitivity to parameter changes. The proposed method and its relevant theoretical framework are validated on an experimental setup with a boost converter prototype and an eZdsp TMS320F2812 processor board.

## 1. Introduction

Because of high demand for renewable-energy (RE) sources, power electronic systems as links between sources, storages, and loads play an increasingly important role in modern power systems [1]. In many RE applications, such as fuel cell and photovoltaic energy systems, the required load voltage is higher than the source voltage. In these cases, boost converters as a small-sized, low-cost, and power-efficient DC-DC converter are of special importance [2]. In addition, many of these RE applications need higher performance power converters with new control strategies. Therefore, any improvement of boost converters' performance such as faster transient response or better response to source voltage and load variations would be beneficial and welcomed in the field of RE systems.

The common approaches to control the boost converter and other DC-DC power converters are based on linearized averaged models and standard frequency-domain design methods [3]. Nonlinear state space-averaged models are also used in many works to achieve better response [3]. An important assumption in the state space-averaging model is that the switching signal varies slowly compared with the changes in state variables [3]. This assumption causes the slow time response of the control method based on the model. Hybrid dynamical system modeling of converters, which directly takes into account the switching nature of the DC-DC converters, promises better transient response and large signal stability [4–9]. A useful outcome of considering the switching nature of DC-DC converters is the time-optimal control (TOC) of the converters [10–12]. Although there has been a vast body of work on TOC of boost converters [10, 13, 14], most of the focus has been on optimization of specific controllers or optimization based on approximate ideal waveforms of the converter [15–17]. Theoretical TOC of buck and boost converters has been done in recent studies [11, 12] using optimal control theory methods like Pontryagin's maximum principle. These researches show that the TOC of buck and boost converters is the minimum switching control based on the bang-bang property [11]. The ideal time-optimal (TO) controller can be implemented using the sliding mode controller (SMC)

framework with switching surfaces based on natural state trajectories. This TO controller has high computational complexity and high sensitivity to circuit parameters [12]. Some linear approximations for this optimal switching surface in the buck converter are proposed to relieve the computational complexity and circuit parameter dependence [7, 13, 16].

Up to date, SMC has been extensively studied [18–22]. Valuable studies are performed on novel sliding surfaces for some applications [23–25]. However, challenges of SMC may not be the same in different application areas. For example, DC-DC converters are switching systems in nature. These systems are designed to achieve desired dynamics by rapidly switching between two or more subsystems. In this case, the control variable is a discrete signal that determines the ON/OFF state of the switches. Hence, the chattering issue in this application is different from the traditional one [23]. The key point to be addressed is finding the time-optimal sliding surface with a stable margin as to relieve the sensitivity to parameter changes [21, 22].

Besides computational complexity and circuit parameter dependence, the traditional time-optimal control of the boost converter has two other important drawbacks. First, high transient current peak may exceed the current limit of the inductor element or the power source. Second, there are higher voltage and current fluctuations around the operating point.

In this paper, the boost converter is modeled as a switched affine (SA) system, and its behavior is studied using the phase portrait. We propose a proximate constrained time-optimal (PCTO) SMC to overcome the shortcomings of the traditional TOC using a piecewise linear switching surface. The proposed method satisfies the reaching and existence conditions of the sliding mode controller, which is visualized by the phase portrait and geometric analysis. The proposed method keeps the inductor current within the determined limits during the transient stage and, at the same time, on the switching surface in the other regions of the state space; the switching surface keeps the state vector on a linear approximation of the ideal switching surface to achieve fast and precise response. The speed response of the proposed method remains close to that of the TOC, while it needs less computational complexity and can be simply implemented using the digital signal processor (DSP). In addition, the performance of the proposed method has less sensitivity to circuit parameter changes.

An experimental prototype based on an eZdsp TMS320F2812 processor board with a sensor and signal conditioning circuit and a boost converter is built to verify our theoretical analysis and effectiveness of the proposed method.

## 2. Boost Converter as a Hybrid Dynamical System

*2.1. Switched Affine Model.* Figure 1 shows a standard boost converter circuit considering the equivalent series resistances (ESRs) of the inductor and capacitor given by $r_L$ and $r_C$, respectively. When the switch $S$ is closed, the current of the inductor increases and energy gets stored in the inductor, and when it is open, the inductor current transfers the stored energy through the diode to the load side. A filter capacitor, $C$, regulates the output voltage to achieve a smooth voltage at the load side.

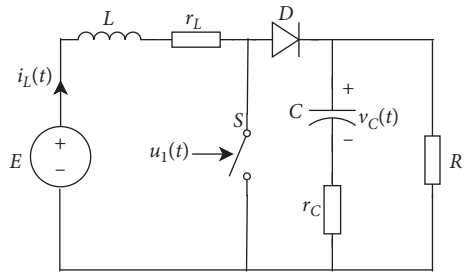


Figure 1: Standard boost converter circuit considering ESRs.

The boost converter shown in Figure 1 has a linear dynamical model for each of the possible configurations of its power electronic switches. This converter has three operation states. In subsystem 1, the switch is ON and the diode is OFF. The dynamics of the system in this state is modeled by

$$x'(t) = f_1(x) = A_1 x + b_1, \tag{1}$$

where

$$A_1 = \begin{bmatrix} \dfrac{-r_L}{L} & 0 \\ 0 & \dfrac{-1}{(R + r_C)C} \end{bmatrix},$$

$$b_1 = \begin{bmatrix} \dfrac{1}{L} \\ 0 \end{bmatrix} E, \tag{2}$$

$$x = \begin{bmatrix} i_L \\ v_C \end{bmatrix}.$$

In subsystem 2, the switch is OFF and the diode is ON. The boost converter is modeled as

$$x'(t) = f_2(x) = A_2 x + b_2, \tag{3}$$

where

$$A_2 = \begin{bmatrix} \dfrac{-1}{L}\left(r_L + \dfrac{r_C R}{(R + r_C)}\right) & \dfrac{-R}{(R + r_C)L} \\ \dfrac{R}{(R + r_C)C} & \dfrac{-1}{(R + r_C)C} \end{bmatrix},$$

$$b_2 = \begin{bmatrix} \dfrac{1}{L} \\ 0 \end{bmatrix} E. \tag{4}$$

Subsystem 3 corresponds to the case when both switches are OFF for which the state space model is as follows:

$$x'(t) = f_3(x) = A_3 x + b_3, \tag{5}$$

where

$$A_3 = \begin{bmatrix} 0 & 0 \\ 0 & \dfrac{-1}{(R + r_C)C} \end{bmatrix}, \qquad b_3 = \begin{bmatrix} 0 \\ 0 \end{bmatrix} E. \tag{6}$$

This model represents a hybrid dynamical system, and its discrete variable can be determined by the switch status and the switching condition of the diode, or simply by its operating state. Although the operating state is both state and input dependent, in many cases, the controller is designed so that mode 3 of operation does not occur corresponding to the continuous conduct mode (CCM) of the converter. In this case, the boost converter model can be simplified to an SA system with two input-dependent operating states:

$$x'(t) = A_q x + b_q, \quad q = 1, 2. \tag{7}$$

This SA system model is used in the following sections to study the boost converter's behavior.

*2.2. Time Response.* Time response for a nonhomogeneous linear system like

$$\begin{cases} x'(t) = Ax + g(t), \\ x(0) = x_0 \end{cases} \tag{8}$$

can be described by

$$x(t) = e^{tA} x_0 + e^{tA} \int_0^t e^{-\tau A} g(\tau) d\tau, \tag{9}$$

where $e^{tA}$ represents the matrix exponential. Each subsystem of the boost converter is a linear nonhomogeneous system similar to (8) with a constant $g$. Therefore, the time response for the state $q$ of the converter is given by

$$x(t) = e^{tA_q} x_0 + e^{tA_q} \int_0^t e^{-\tau A_q} b_q d\tau. \tag{10}$$

Since $A^{-1}$ and $A$ commute, using matrix exponential properties, we have

$$x(t) = e^{tA_q} x_0 + e^{tA_q} A_q^{-1} b_q - A_q^{-1} b_q. \tag{11}$$

Finally, in each subsystem, the boost converter's time response is represented as follows:

$$x(t) = e^{tA_q}(x_0 - x_e) + x_e, \quad x_e = A_q^{-1} b_q. \tag{12}$$

For $t = 0$, the matrix exponential equals the identity matrix, so the initial condition is satisfied. If the eigenvalues of $A_q$ have negative real parts, the matrix exponential will converge to the zero matrix as $t$ goes to infinity. In that case, the equilibrium of the boost converter is

$$x_e = A_q^{-1} b_q. \tag{13}$$

The state matrix $A_1$ has two real eigenvalues, implying that the equilibrium point is a simple node. The eigenvalues of $A_2$ are two complex numbers with negative real parts; hence, the equilibrium point is a spiral asymptotically stable point. The above equations are used for the phase portrait of the boost converter in its different operating modes in the following sections.

*2.3. Phase Portrait Representation.* Phase portrait representations for a boost converter with the second circuit parameter set given in Table 1 are depicted in Figure 2. In this section, circuit 1 is used for better representation of the boost converter's state trajectories in its different operating subsystems. In the remaining parts of this paper, specifications of circuit 2 in Table 1 are used in all simulation and experimental tests.

As can be seen in Figure 2, in subsystem 1, each of the state trajectories converges to a point on the $i_L$ axis. Subsystem 2 has a spiral stable point in the middle of the continuous state space. The control input of a boost converter is a discrete switching signal which turns the switch ON or OFF. Fast switching between two phase portraits with varying average dwell time results in custom state trajectories in the continuous state space. Figure 2(c) shows a sample state trajectory for the fixed PWM input with 35% of duty cycle. To better illustrate the switching effect, the carrier frequency is kept low in this PWM signal.

Figure 2(c) also depicts the possible equilibrium points of the converter state vector. To have closed-loop stability in a boost converter control system, the desired state values cannot be arbitrary points on the continuous state space. To hold the state trajectory in a neighborhood around a desired point, there should be a suitable switching sequence which moves the states in a limit cycle around the desired point. These possible equilibrium points form a conic section in the continuous state space and can be calculated by simulating the PWM signals with different duty cycles. The result of this simulation is shown in Figure 2(c).

## 3. Time-Optimal Control

In [15], it is shown using Pontryagin's maximum principle that time-optimal control of a boost converter is a bang-bang control, and it is proved that this time-optimal control is also minimum switching control [7]. In a physical sense, when the load resistance steps up, the controller should turn the switch ON to store sufficient energy in the inductor. The controller will turn the switch OFF when the state variables reach a special trajectory of the switch OFF mode. This trajectory will reach the desired state variable point. Then, the controller will keep the state variables near the desired point. This time-optimal control can be implemented as a sliding mode controller whose switching surface is defined

Table 1: Specifications of used boost converters.

| Description | Circuit 1 | Circuit 2 | Parameter |
|---|---|---|---|
| Nominal input | 20 V | 5 V | $V_S$ |
| Desired output | 30 V | 15 V | $V_O$ |
| Load resistance | 10 Ω | 112 Ω | $R$ |
| Inductance | 700 $\mu$H | 128 $\mu$H | $L$ |
| Inductor DCR | 0.4 Ω | 0.2 Ω | $r_L$ |
| Capacitance | 15 $\mu$F | 470 $\mu$F | $C$ |
| Capacitor ESR | 0.2 Ω | 0.5 Ω | $r_C$ |

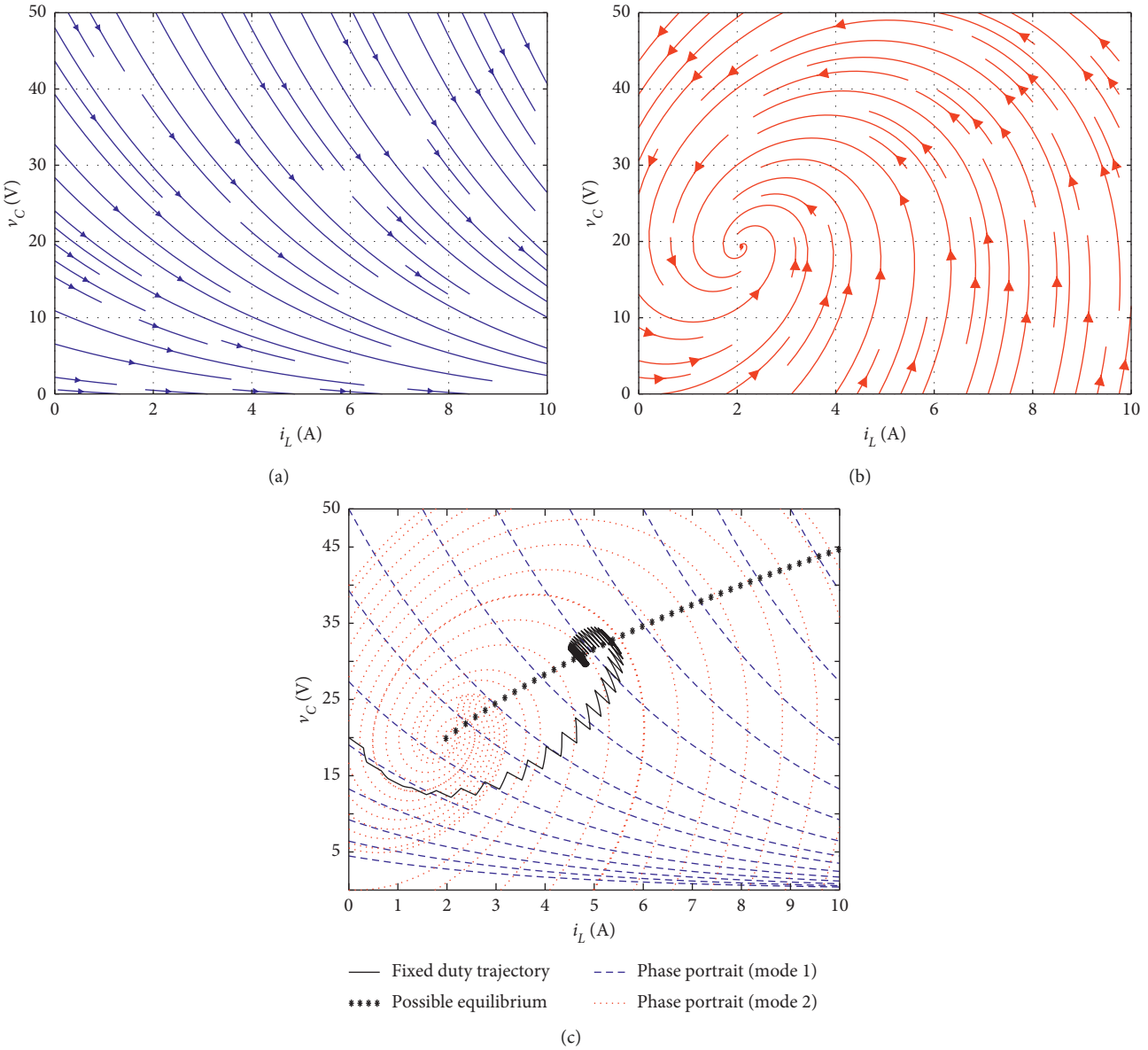


Figure 2: Phase portrait representation of system behavior. (a) Phase portrait of mode 1. (b) Phase portrait of mode 2. (c) Fixed duty cycle trajectory.

by combining two natural state trajectories of subsystem 1 and subsystem 2 of the boost converter [6].

Figure 3 shows an ideal state trajectory for time-optimal control of a boost converter with specifications of circuits given in Table 1. Voltage and current waveforms of the ideal time-optimal controller are depicted in Figure 3. Despite the fast response time, this time-optimal controller has the following four major drawbacks:

(1) High computational complexity

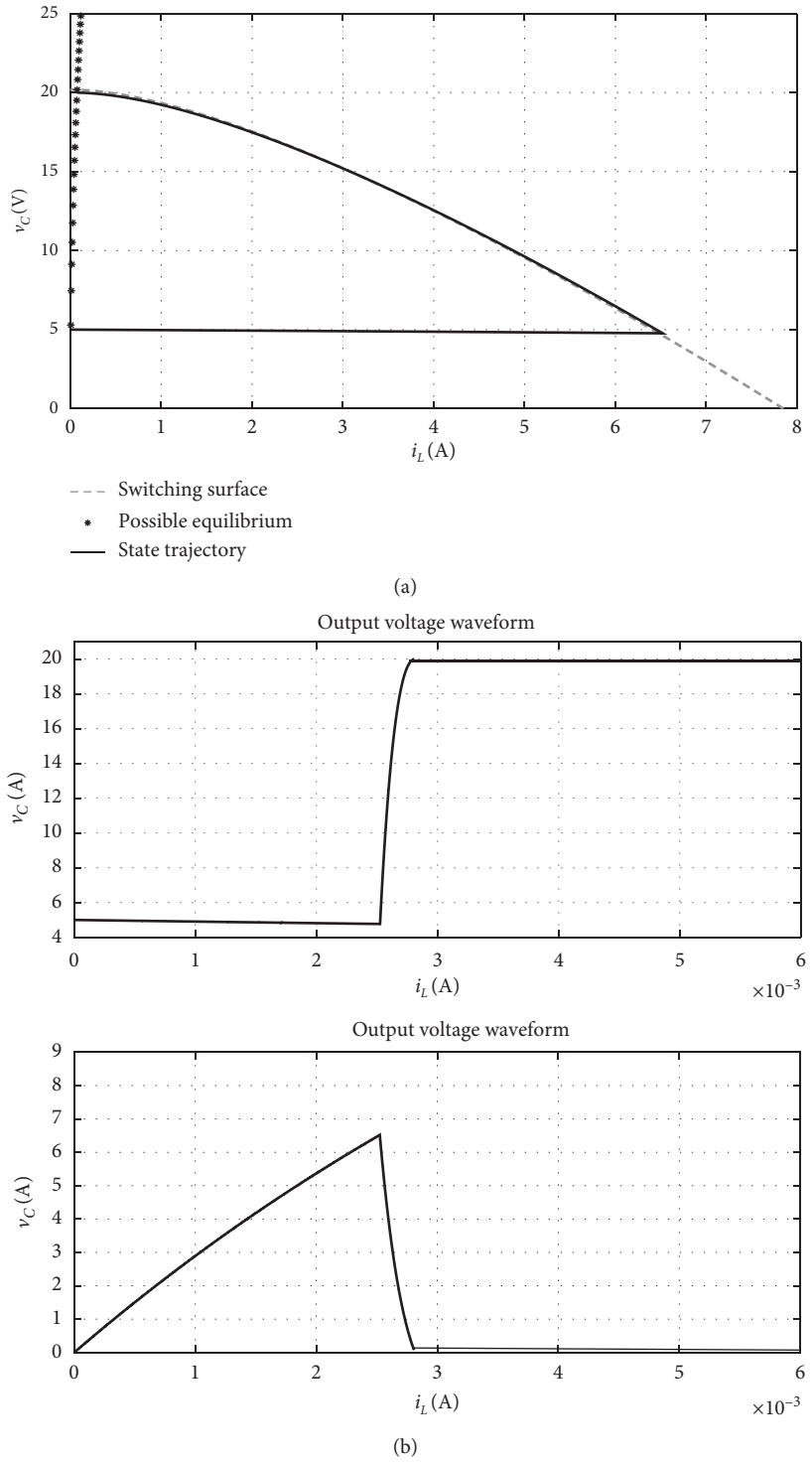


Figure 3: Ideal TOC: (a) state trajectory; (b) waveforms.

(2) Circuit parameter dependence

(3) Big transient current overshoot

(4) High steady-state voltage ripples

Although the simulated waveforms show good steady-state operation, in experimental tests, high current and voltage fluctuations will occur because of the aligned direction of the switching surface and trajectories.

Linear approximations of the optimal state trajectories can be used to overcome the first issue highlighted above and to some extent the second issue. In this paper, a conventional sliding mode controller is tuned to reduce the current overshoot within the determined limits. Then, to improve the response time, we investigate piecewise linear switching surfaces to maintain the inductor current within its allowed maximum designed value.

## 4. Tuned SMC

*4.1. Sliding Mode Control Principle.* In this section, a conventional SMC is tuned to keep the boost converter's response time low while maintaining the current limit. In the SMC, the system state trajectory first moves toward a surface in the state space, namely, the sliding surface. Second, the system state slides near the surface and converges to a desired equilibrium point (8) [14]. The first and second parts of the SMC state trajectory are called the reaching mode and sliding mode, respectively (8). The design procedure of an SMC has two major steps. In the first step, a switching surface is defined which has the desired convergence properties and provides the required asymptotic behavior. In the second step, a switching law is designed so that the reaching condition is guaranteed.

*4.2. Sliding Surface Definition.* The sliding surface of a conventional SMC for the boost converter can be defined as

$$S = k\left(i_L - i_{\text{ref}}\right) + \left(v_C - v_{\text{ref}}\right) = \begin{bmatrix} k \\ 1 \end{bmatrix}^T \left(x - x_r\right), \tag{14}$$

where $x_r = [i_{\text{ref}}, v_{\text{ref}}]^T$ and $v_{\text{ref}}$ and $i_{\text{ref}}$ are the desired output voltage and inductor current, respectively. The desired output voltage is determined by the specification of applications; the desired inductor current is determined by both the desired output voltage and the switching law.

The corresponding switching law for the defined sliding is

$$q = \begin{cases} 1, & S \le 0, \\ 2, & S > 0, \end{cases} \tag{15}$$

where $q$ is the index for subsystems defined in Section 2.

*4.3. Existence Condition.* The existence condition for the sliding surface guarantees that there exists a region near the sliding surface, in which the switching law can steer each initial state inside it to hit the sliding surface. This condition is formulated as

$$\exists \varepsilon > 0 \text{ satisfying} \begin{cases} S' > 0, & \text{for } -\varepsilon < S < 0, \\ S' < 0, & \text{for } 0 < S < \varepsilon. \end{cases} \tag{16}$$

This condition guarantees that, in some regions around the surface, the switching law steers state variables toward them. According to (1), (3), (15), and (16), the time derivative $S'$ is

$$S' = \sum \frac{dS}{dx_i}\frac{dx_i}{dt} = \nabla S \cdot x' = \begin{cases} S_1' = \begin{bmatrix} k \\ 1 \end{bmatrix}^T f_1(x), & S < 0, \\ S_2' = \begin{bmatrix} k \\ 1 \end{bmatrix}^T f_2(x), & S > 0. \end{cases} \tag{17}$$

Since state transition functions of both modes are continuous, $S_1'$ and $S_2'$ are continuous. Hence, for the existence condition, it is sufficient that

$$S_1'\big|_{S=0} > 0 \wedge S_2'\big|_{S=0} < 0, \tag{18}$$

where $\wedge$ represents intersection and

$$\begin{cases} S_1' = \begin{bmatrix} k \\ 1 \end{bmatrix}^T f_1(x) = \begin{bmatrix} k \\ 1 \end{bmatrix}^T . \left(A_1 x + b_1\right), \\ S_2' = \begin{bmatrix} k \\ 1 \end{bmatrix}^T f_2(x) = \begin{bmatrix} k \\ 1 \end{bmatrix}^T . \left(A_2 x + b_2\right). \end{cases} \tag{19}$$

Condition $S = 0$ in (18) makes $i_L$ and $v_C$ dependent so that the inequalities are functions of $i_L$ and $k$. For an ideal boost converter without parasitic elements, the existence of inequalities (17) can be solved to derive limitations for the parameter $k$ factor. However, when parasitic elements exist, these inequalities are expanded as follows.

*Inequality 1*

$$S_1' = P_1 k i_L + P_2 k + P_3 > 0, \tag{20}$$

where

$$\begin{aligned} P_1 &= \frac{P_3}{v_{\text{ref}}} - \frac{r_L}{L}, \\ P_2 &= \frac{v_s}{L} - \frac{P_3 i_{\text{ref}}}{v_{\text{ref}}}, \\ P_3 &= \frac{v_{\text{ref}}}{C\left(R + r_C\right)}. \end{aligned} \tag{21}$$

*Inequality 2*

$$S_2' = Q_1 k^2 i_L + Q_2 k^2 + Q_3 k i_L + Q_4 k + Q_5 i_L + Q_6 < 0, \tag{22}$$

where

$$\begin{aligned} Q_1 &= \frac{R}{L\left(R + r_C\right)}, \\ Q_2 &= -Q_1 * i_r, \\ Q_3 &= \frac{-r_L}{L} - r_C Q_1 + \frac{Q_5}{R}, \\ Q_4 &= \frac{E}{L} - Q_1 * v_r + Q_6 * \frac{i_r}{v_r}, \\ Q_5 &= Q_1 * \frac{L}{C}, \\ Q_6 &= -Q_5 * \frac{v_r}{R}. \end{aligned} \tag{23}$$

It can be shown analytically that inequality 1 holds for positive values of $i_L$ and $k$. But $S_2'$ in inequality 2 has a third-order two-variable function, and it is better to solve it numerically. Figure 4 depicts a contour plot for $S_1'$ and $S_2'$

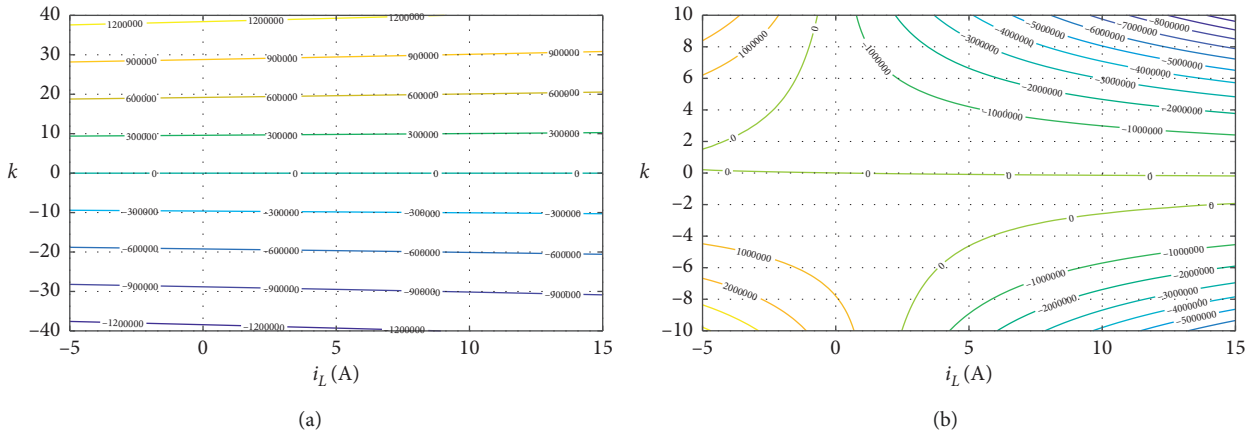


Figure 4: Contour plot for existence condition inequalities. (a) Contour plot for inequality 1. (b) Contour plot for inequality 2.

with respect to $k$ and $i_L$ for a sample boost converter with circuit 1 parameters given in Table 1.

According to (18), $S_1'$ should be greater than zero. Figure 4 shows that there are no limitations when $i_L$ and $k$ are positive. According to (18), $S_2'$ should be smaller than zero. For every positive value of $k$, there is a minimum value of $i_L$ for $S_2'$ to be positive. The zero level of the contour determines this limit.

*4.4. Reaching Condition.* The existence condition guarantees sliding and remaining on the surface when the state is near the defined sliding surface, but the reaching condition guarantees that when the initial state is far from the sliding surface, it will reach the surface in finite time. The reaching condition of states to the surface is simply proved according to the time response of the converter in (11). From this equation, it can be concluded that as long as the eigenvalues of state matrices have negative real parts, the trajectory will converge to $x_e$ for different subsystems:

$$\lim_{t\longrightarrow\infty} x(t) = x_{e_q} = \begin{cases} -A_1^{-1}b_1, & q = 1, \\ -A_2^{-1}b_2, & q = 2. \end{cases} \tag{24}$$

According to the switching rule in (15), the switch will be ON when $S < 0$ and OFF when $S > 0$; then, all trajectories will reach the sliding surface if the following conditions are met:

$$\begin{cases} \text{if } (x_{e_1}) > 0, \\ \text{if } (x_{e_2}) < 0. \end{cases} \tag{25}$$

This reaching condition can be properly interpreted in the phase portrait.

It can be proved that if the equilibrium point of one subsystem is located in the opposite region where the other subsystem works, then the reaching condition is satisfied. Figure 5 depicts a representation of this condition.

*4.5. Sliding Dynamics.* The equivalent dynamics of the system on the sliding surface will steer the state toward the desired state. Suppose that the system state is on the surface

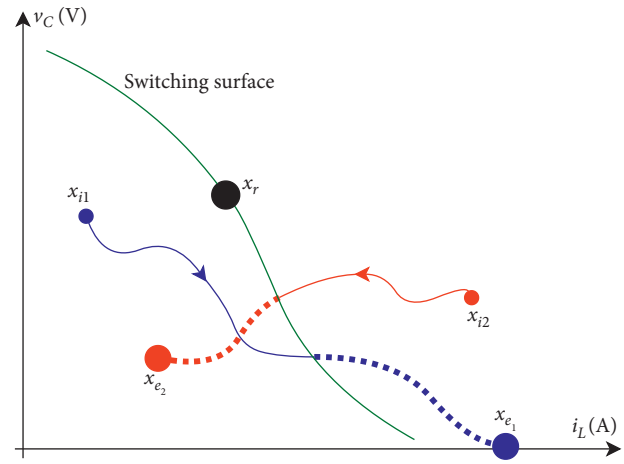


Figure 5: Reaching condition of the SMC.

and slides on it, then the equivalent time derivative of $S$ should be zero. From (19), we have

$$\begin{cases} S = \begin{bmatrix} k \\ 1 \end{bmatrix}^T (x - x_r) = m^T (x - x_r) = 0, \\ S_{e_q}' = [S_1', S_2'] \cdot r = m^T [f_1(x), f_2(x)] \cdot r = 0, \end{cases} \tag{26}$$

where $m$ is the slope and $r$ is a vector which plays a role similar to the duty cycle in PWM switching. A candidate solution to $r$ will be defined as

$$r = \begin{bmatrix} -f_2 \\ f_1^T \end{bmatrix} m. \tag{27}$$

Sliding dynamics of the system is the dynamics of the state variable on the sliding surface. A measure of the state variable position on the sliding surface is defined by

$$D = \begin{bmatrix} -1 \\ k \end{bmatrix}^T (x - x_r) = n^T (x - x_r), \tag{28}$$

where $n$ is a vector perpendicular to $m$ and parallel to the surface. Therefore, the sliding dynamics will be the time derivative of this defined position:

$$D' = n^T [f_1(x), f_2(x)] r = n^T [f_1(x), f_2(x)] \begin{bmatrix} -f_2^T \\ f_1^T \end{bmatrix} m,$$
$$D' = \|m\|^2 \times \det[f_1(x), f_2(x)]. \tag{29}$$

But the above determinant is positive below the conic section of possible equilibrium points and negative above it. Since $R$ is positive above $x_r$ and above the conic section for positive $k$ values, we have

$$D \times D' < 0, \quad \text{for all } x \text{ on } S = 0. \tag{30}$$

Therefore, the system state converges to $x_r$ for any initial state.

*4.6. Simulation of Tuned SMC.* The performance of the tuned conventional SMC is simulated using the MATLAB software. Figure 6 shows the state trajectory and waveforms for the sample boost converter. This SMC reduces the transient current overshoot and can be simply implemented. However, voltage and current waveforms show that the time response is slow compared with the time-optimal control. Another drawback of this controller is the output voltage dependent on circuit parameters.

## 5. Proximate Constrained Time-Optimal SMC

*5.1. Principle of Operation.* Although the tuned conventional SMC takes care of the inductor current limit and has an acceptable response speed, the conventional controller may not be the fastest controller with this determined constraint. To achieve the fastest possible response, it is necessary to hold the converter's current in its maximum allowed value during the transient. This idea leads to a constrained TOC. But TOC has a high computational complexity again. In this section, a modified piecewise linear switching surface will be defined. This modified surface keeps the inductor current high enough in the transient state, and then the system state converges to its desired value in a suitable manner near the time-optimal trajectory. This method keeps the response speed as fast as possible and the steady-state voltage oscillations as low as possible.

*5.2. Piecewise Sliding Surface.* The new piecewise switching surface of the proposed SMC is defined as

$$S = \begin{cases} k(i_L - i_{\text{ref}}) + (v_C - v_{\text{ref}}), & i_L < i_{\max}, \\ (i_L - i_{\max}), & i_L \geq i_{\max}, \end{cases} \tag{31}$$

where $i_{\max}$ represents the maximum allowed inductor current. In (31), $k$ is a positive factor but has small values to keep the time response fast.

*5.3. Existence Condition.* The existence condition for the first part of the new sliding surface is similar to that of the conventional SMC, but for the second part corresponding to a constant-current region, it is investigated as follows. The derivative of the surface function for the constant-current region is

$$S'_{CC1}\big|_{S=0} > 0 \wedge S'_{CC2}\big|_{S=0} < 0, \tag{32}$$

where

$$S'_{CC} = \begin{cases} S'_{CC1} = \begin{bmatrix} 1 \\ 0 \end{bmatrix}^T f_1(x), & S < 0, \\ S'_{CC2} = \begin{bmatrix} 1 \\ 0 \end{bmatrix}^T f_2(x), & S > 0. \end{cases} \tag{33}$$

Condition $S = 0$ in (32) makes $i_L$ and $v_C$ dependent so that the inequalities are functions of $i_L$ and $k$. Therefore, the inequalities can be expanded as follows.

*Inequality 3*

$$S'_{CC1} = \frac{-r_L i_L}{L} + \frac{v_s}{L} > 0, \quad i_L = \underset{\rightarrow}{i}_{\max} i_{\max} < \frac{v_s}{r_L}. \tag{34}$$

Since $r_L \ll 1$, this inequality is true in most practical cases. The second inequality can be derived as follows.

*Inequality 4*

$$S'_2 = \frac{-i_L}{L}\left(r_L + \frac{Rr_C}{R + r_C}\right) + \frac{-Rv_C}{L(R + r_C)} + \frac{v_s}{L} < 0, \tag{35}$$

$$v_C > v_s\left(\frac{R + r_C}{R}\right) - i_{\max}\left(\frac{r_L(R + r_C)}{R} + r_C\right). \tag{36}$$

Assume that $r_o \gg r_C$, then (36) becomes

$$v_C > v_s - i_{\max}(r_L + r_C)r_L, \quad r_C \ll \underset{\longrightarrow}{1} \; v_C > v_s. \tag{37}$$

This inequality guarantees that if the initial voltage is greater than the source voltage, the output current can slide on the constant-current switching surface, and it will not exceed it. But when the initial voltage is much lower than the source voltage, the converter may exceed the maximum current limits. It can be seen in the phase portrait of the vector fields that this is a natural property of the boost converter and does not belong to the proposed controller. To overcome this overcurrent problem for small initial voltages, it is suitable to start the converter with a startup higher resistance load and then switch to the full load.

*5.4. Reaching Condition.* Reaching condition can be proved similarly to the conventional SMC case. Since the equilibrium point of subsystem 1 is in the opposite side of the switching surface, any trajectory starting from the subsystem 1 side will hit the sliding surface. This is true for trajectories starting from the subsystem 2 side, similarly.

*5.5. Sliding Dynamics.* Sliding dynamics for the first part of the surface is exactly the same as that of the conventional SMC. For the constant-current part, the following definitions lead to a similar proof:

$$m = [1, 0]^T,$$
$$n = [0, 1]^T, \tag{38}$$
$$D = n^T(x - x_s),$$

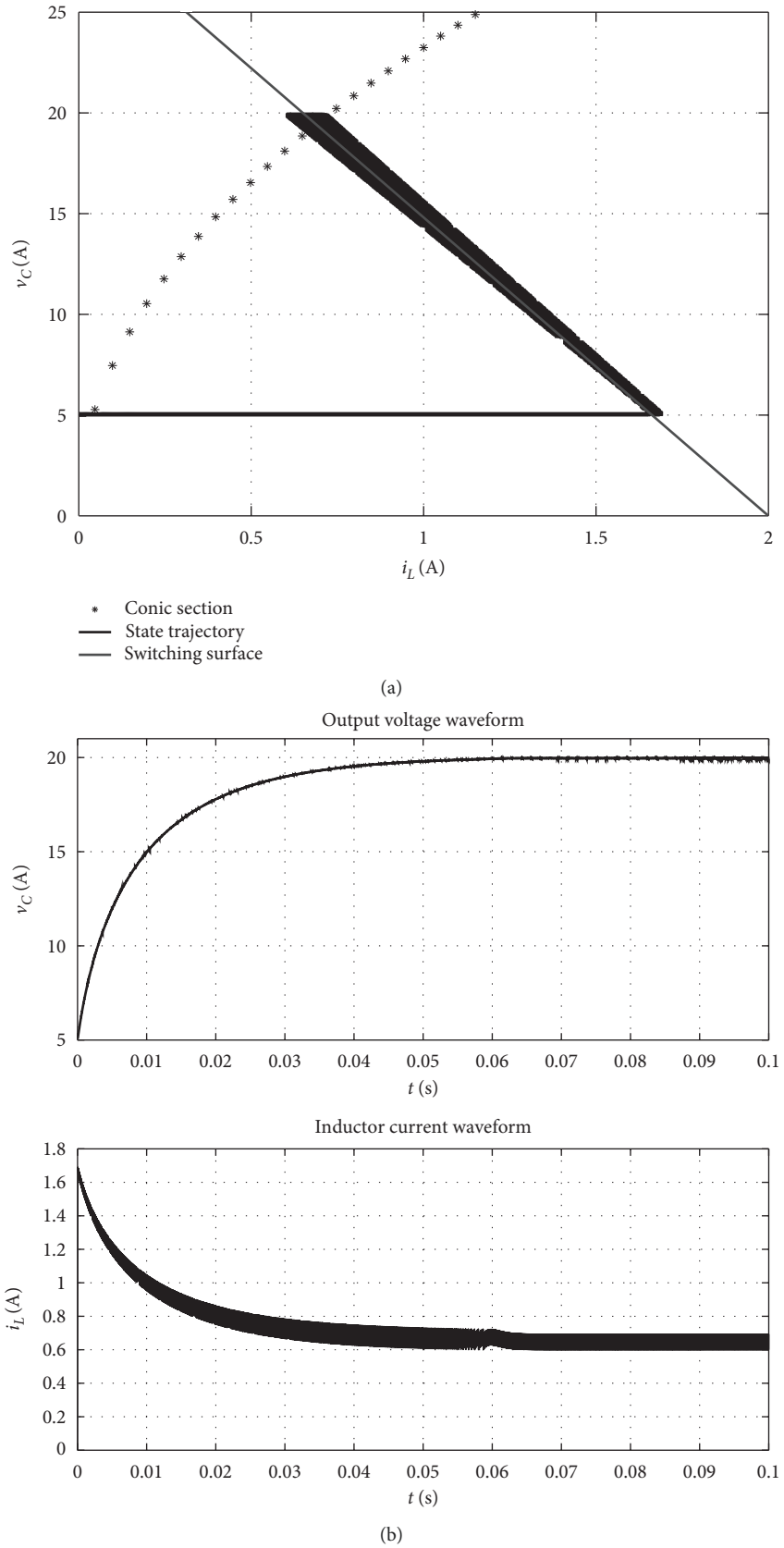


Figure 6: (a) State trajectory and (b) waveforms of the tuned SMC.

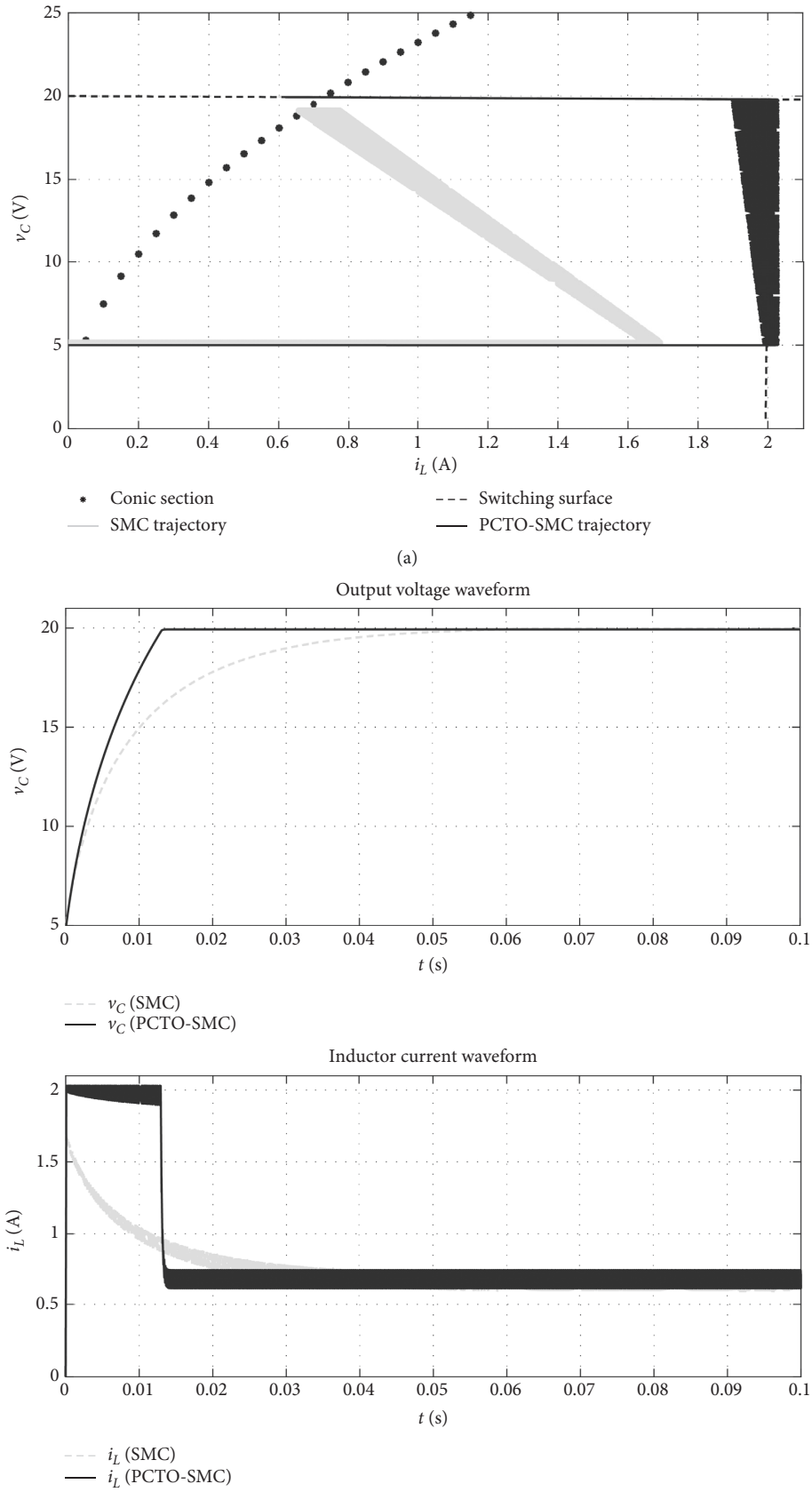


Figure 7: (a) State trajectory and (b) waveforms of the PCTO-SMC.

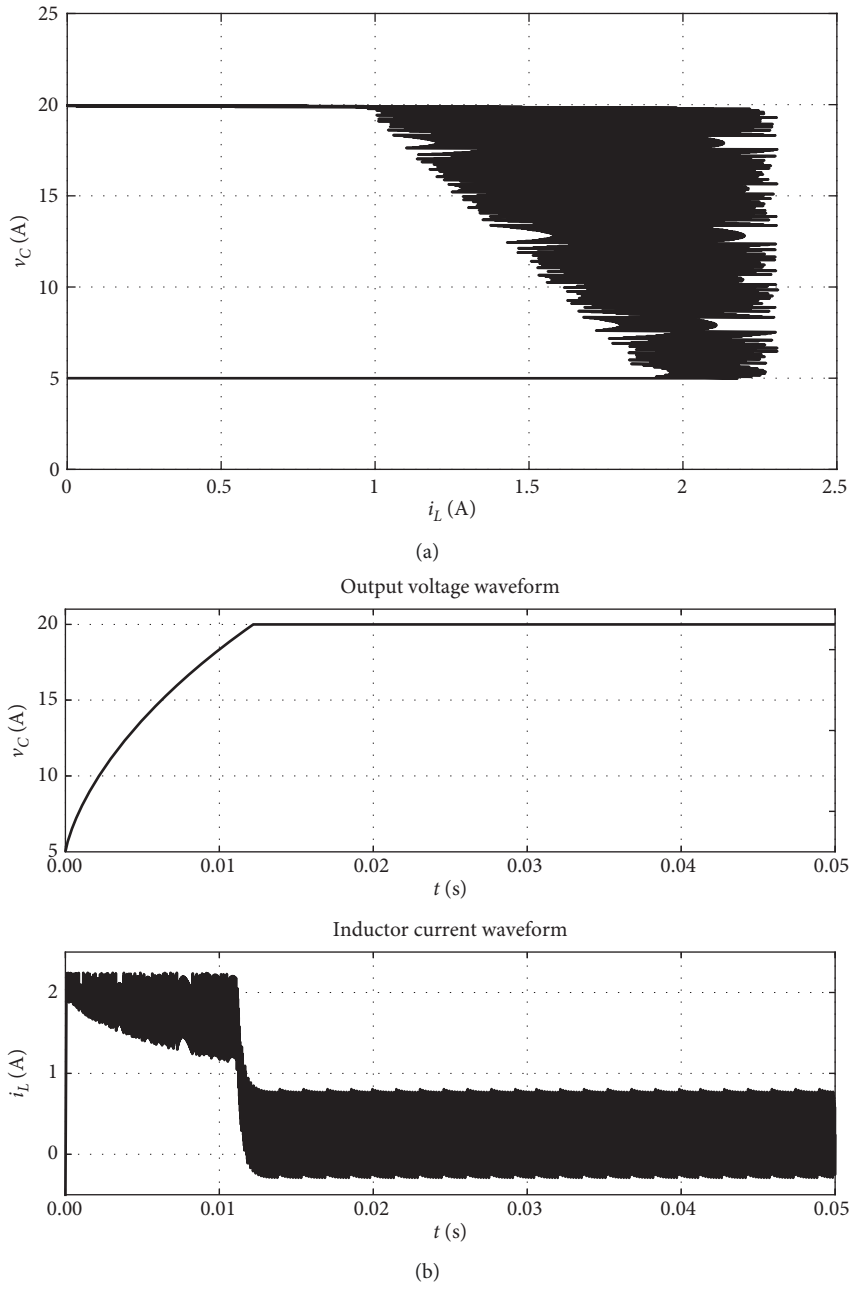


Figure 8: (a) State trajectory and (b) waveform simulations of the PCTO-SMC ($T_s = 10\,\mu$s).

where $x_s$ is the intersection of the constant-current line with the conic section. Using these definitions, it can be shown that if the system state reaches the constant-current surface, it will slide up to the corner of the two switching surfaces and then toward the desired state.

*5.6. Simulation of the Proposed Controller.* Simulation results of the proposed PCTO-SMC for circuit 2 parameters given in Table 1 are shown in Figure 7. These simulation results show that the proposed controller has a faster time response and a voltage rise time of about 17 ms which is a better result as compared to the conventional SMC with about 40 ms rise time.

*5.7. Controller Parameters.* The switching surface of (31) can be simply implemented by DSP-based controllers. The controller parameters include $i_{\text{ref}}$, $v_{\text{ref}}$, $i_{\max}$, and $k$. The $k$ parameter determines the slope of the near-optimal part of the switching surface. In practice, since $r_l, r_c \ll 1$, the existence condition, (20) and (22), can be simplified as $k > k_{\min}$ where $k_{\min} = L \cdot v_{\text{ref}}/(R \cdot C \cdot v_s)$ is the slope of the time-optimal switching surface and has a small positive value. For example,

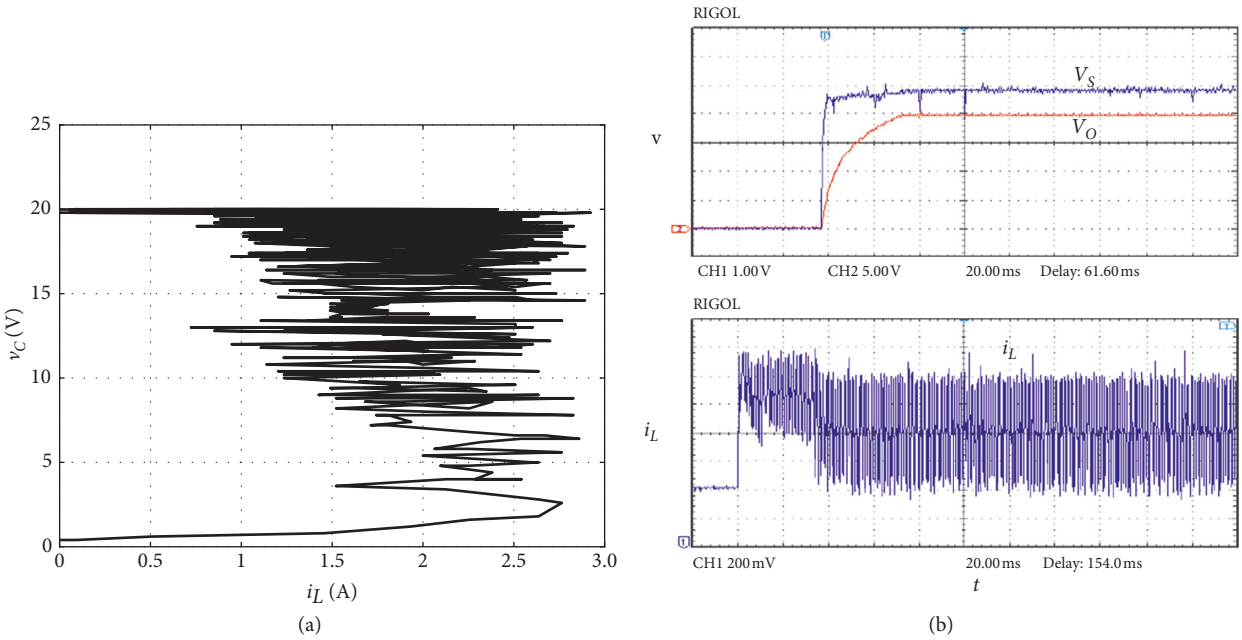


Figure 9: Experiment: (a) state trajectory; (b) waveforms.

for circuit 2 parameters given in Table 1, $k_{\min} = 0.007$. Hence, as long as $k$ is near $k_{\min}$, the controller's response speed remains close to that of the time-optimal controller. On the contrary, when $k$ is very close to $k_{\min}$, the controller has a marginal behavior in sliding existence and stability.

The $v_{\text{ref}}$ parameter is the desired output voltage which is an input to the controller in DC-DC converters. The $i_{\text{ref}}$ parameter is dependent on $v_{\text{ref}}$ and can be approximated by $v_{\text{ref}} \approx v^2/(R \cdot v_s)$. However, in practice, because of low values of $k$, selecting $i_{\text{ref}} = 0$ in (31) gives rise to less than 0.1% error in the output voltage. Hence, the switching surface can be simplified by removing $i_{\text{ref}}$ in (31).

## 6. Experimental Validation

*6.1. State Trajectory and Startup.* Simulation results in the previous sections show faster time response for the proximate constrained time-optimal SMC. But the other capabilities of this controller, which are proved in previous sections, are better illustrated in experimental results. The proposed controller's performance is validated in the laboratory using a prototype boost converter with the parameters of circuit 2 in Table 1. An eZdsp F2812 board is used to implement the controller.

Because of switching frequency limitations, the sample time of the eZdsp board is set to 10 $\mu$s. This sample time causes higher current fluctuations in the state trajectory and current waveforms. Therefore, for comparison with the experimental waveforms, simulation results with the practical sampling frequency will be compared here. Figure 8 shows the state trajectory and waveforms of the PCTO-SMC with 10 $\mu$s sample time and 5 V source voltage and 20 V desired output voltage starting from an initial voltage of 5 V. It is shown in these simulations that, with larger sample time, the converter's current ripple will be higher. The corresponding experimental results for voltage and current waveforms are shown in Figure 9. The state trajectory is exported to the personal computer using the Oscilloscope software tool and then plotted in Figure 9. It is depicted in this figure that the experimental validation has similar results to the previous simulations. The reminder of this section shows the experimental results related to changes in load, source voltage, and output voltage reference.

*6.2. Response to Load, Source Voltage, and Reference Voltage Changes.* Several experimental tests were carried out to investigate the controller's response to the load resistance, source voltage, and reference output changes. Possible changes of load between $R = 112\,\Omega$ and $R = 56\,\Omega$ and between $R = 112\,\Omega$ and $R = 232\,\Omega$ have been tested. Figure 10 shows some of these results. Output voltage varies about 1% of its nominal voltage in response to load changes. Note that sensitivity to the load changes can be further reduced by tuning the switching surface slope $k$. Reducing the $k$ parameter leads to smaller output voltage variations but more current fluctuations. Current fluctuations can be reduced again by increasing the switching speed (corresponding to shortening the sampling time). This is not possible in the present experimental setup.

Source voltage changes between 1.5 V, 3.3 V, 5 V, and 10 V have been tested. Figure 10(c) shows output voltage response when the source voltage changes from 10 V to 5 V. The results show less than 0.5% of nominal value changes in the output voltage. Several experimental tests for step changes in the reference voltage were also performed. Figure 10(d) shows output voltage and inductor current response to reference voltage changes between 10 V and 20 V. Experimental results show about 20 ms rise time and 40 ms fall time in the output voltage waveform.

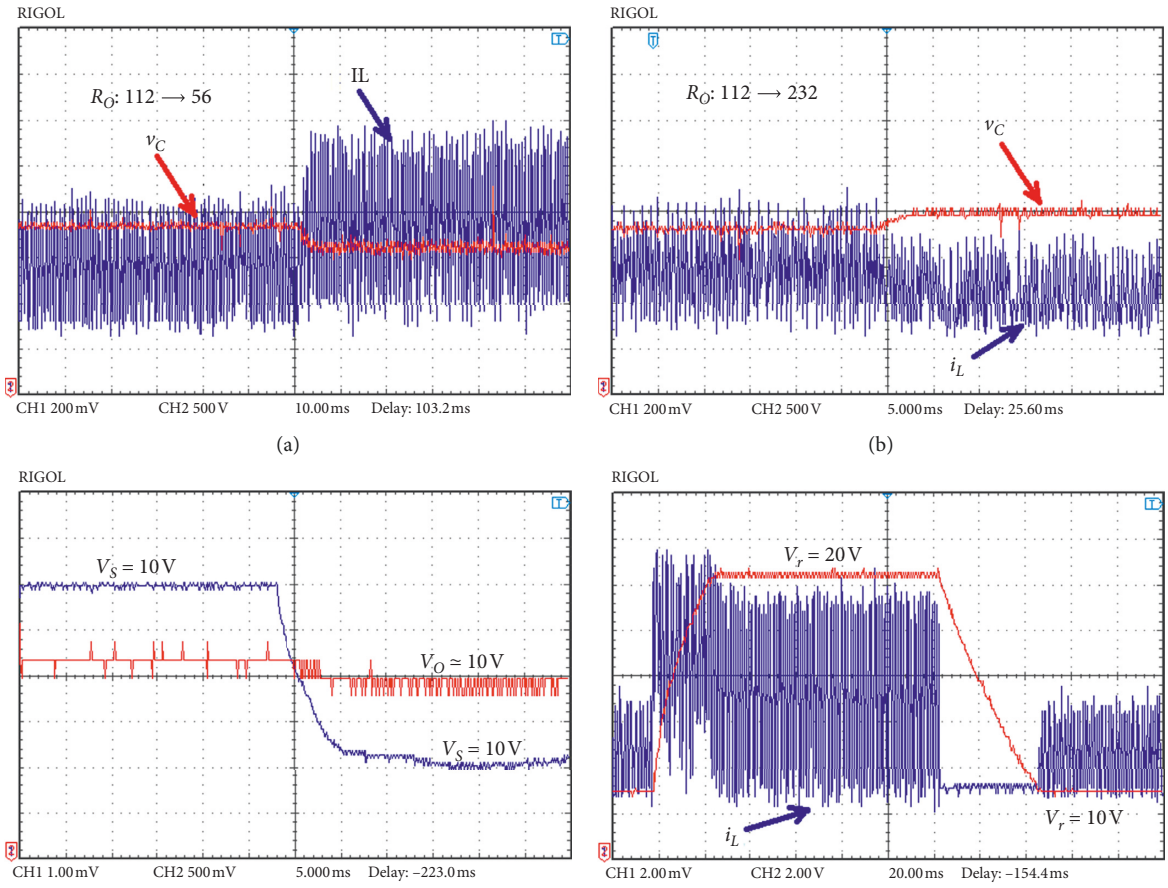


FIGURE 10: Experimental results of voltage and current response to load, source voltage, and reference voltage changes. (a) Response 1 to $R_O$ change. (b) Response to $V_S$ change. (c) Response 2 to $R_O$ change. (d) Response to $V_r$ change.

## 7. Conclusion

A hybrid switching system model of the boost converter and phase portrait geometric representation of the corresponding vector fields lead to better description of its behavior. Then, a new proximate constrained time-optimal sliding mode controller is proposed which directly controls the converter switch. This controller has faster response time compared to conventional SMC. The proposed method has a current limitation capability by designing a piecewise sliding surface to maintain the inductor current constraint. Experiment results show good response to changes in load resistance, source voltage, and output voltage reference. Limited current and low output variation in load and source variations are beneficial in many RE applications. Compared to the time-optimal control, the proposed controllers achieve much lower current peak and steady-state voltage fluctuations and also lower computational complexity.

## Data Availability

The MATLAB file data used to support the findings of this study are available from the corresponding author upon request.

## Conflicts of Interest

The authors declare that they have no conflicts of interest.

## Acknowledgments

This paper was supported in part by the Shaanxi Provincial Special Support Program for Science and Technology Innovation Leader and in part by the Shaanxi Industrial Key Project (2018GY-165).

## References

[1] J. M. Carrasco, L. G. Franquelo, J. T. Bialasiewicz et al., "Power-Electronic systems for the grid integration of renewable energy sources: a survey," *IEEE Transactions on Industrial Electronics*, vol. 53, no. 4, pp. 1002–1016, 2006.

[2] İ. Yazici and E. K. Yaylaci, "Fast and robust voltage control of DC–DC boost converter by using fast terminal sliding mode controller," *IET Power Electronics*, vol. 9, no. 1, pp. 120–125, 2016.

[3] R. D. Middlebrook and S. Cuk, "A general unified approach to modelling switching-converter power stages," in *Proceedings of the Power Electronics Specialists Conference*, Cleveland, OH, USA, 1976.

[4] T. A. F. Theunisse, J. Chai, R. G. Sanfelice, and W. P. M. H. Heemels, "Robust global stabilization of the DC-DC boost converter via hybrid control," *IEEE Transactions on Circuits and Systems I: Regular Papers*, vol. 62, no. 4, pp. 1052–1061, 2015.

[5] H. Molla-Ahmadian, F. Tahami, A. Karimpour, and N. Pariz, "Hybrid control of DC–DC series resonant converters: the direct piecewise affine approach Approach," *IEEE Transactions on Power Electronics*, vol. 30, no. 3, pp. 1714–1723, 2015.

[6] S. A. Evangelou and M. A. Rehman-Shaikh, "Hybrid electric vehicle fuel minimization by DC-DC converter dual-phase-shift control," *Control Engineering Practice*, vol. 64, pp. 44–60, 2017.

[7] H.-P. Ren, X. Guo, Y.-C. Zi, and J. Li, "Double loop control of boost converter based current switching controller and voltage compensator," in *Proceedings of 7th International Conference on Electronics, Computers and Artificial Intelligence (ECAI)*, pp. E11–E16, Bucharest, Romania, June, 2015.

[8] H.-P. Ren, M.-M. Zheng, and J. Li, "A simplified mixed logical dynamic model and model predictive control of boost converter with current reference compensator," in *Proceedings of the 2015 IEEE 24th International Symposium on Industrial Electronics (ISIE)*, pp. 61–65, Armação dos Búzios, Brazil, June, 2015.

[9] J. Li, T. Zheng, and H.-P. Ren, "Method of increasing the output voltage precision for switching control of power converter," Patent in China, No. 201210093047, 2014.

[10] C. Olalla, I. Queinnec, R. Leyva, and A. El Aroudi, "Robust optimal control of bilinear DC-DC converters," *Control Engineering Practice*, vol. 19, no. 7, pp. 688–699, 2011.

[11] J. Nazarzadeh and M. J. Jafarian, "Applying bilinear time-optimal control system in boost converters," *IET Power Electronics*, vol. 7, no. 4, pp. 850–860, 2014.

[12] M. Jafarian and J. Nazarzadeh, "Time-optimal sliding-mode control for multi-quadrant buck converters," *IET Power Electronics*, vol. 4, no. 1, pp. 143–150, 2014.

[13] E. Meyer, Z. Zhang, and Y.-F. Liu, "Digital charge balance controller to improve the loading/unloading transient response," *IEEE Transactions On Power Electronics*, vol. 27, no. 3, pp. 1314–1326, 2012.

[14] C. Olalla, I. Queinnec, R. Leyva, and A. El Aroudi, "Optimal state-feedback control of bilinear DC–DC converters with guaranteed regions of stability," *IEEE Transactions On Industrial Electronics*, vol. 59, no. 10, pp. 3868–3880, 2012.

[15] W. Feng, F. C. Lee, and P. Mattavelli, "Optimal trajectory control of LLC resonant converters for LED PWM dimming," *IEEE Transactions On Power Electronics*, vol. 29, no. 2, pp. 979–987, 2014.

[16] S. Kapat and P. T. Krein, "Improved time optimal control of a buck converter based on capacitor current," *IEEE Transactions On Power Electronics*, vol. 27, no. 3, pp. 1444–1454, 2012.

[17] L. Corradini, A. Babazadeh, A. Bjeleti´, and D. Maksimović, "Current-limited time-optimal response in digitally controlled DC–DC converters," *IEEE Transactions On Power Electronics*, vol. 25, no. 11, pp. 2869–2880, 2012.

[18] V. Utkin, "Variable structure systems with sliding modes," *IEEE Transaction on Automatic Control*, vol. 22, no. 2, pp. 212–222, 1977.

[19] R. A. DeCarlo, S. H. Zak, and G. P. Mathews, "Variable structure control of nonlinear multivariable systems: a tutorial," *Proceedings of the IEEE*, vol. 76, no. 3, pp. 212–232, 1988.

[20] Y. Shtessel, C. Edwards, L. Fridman, and A. Levant, *Sliding Mode Control and Observation*, Springer, Berlin, Germany, 2014.

[21] S.-N. Mirebrahimi, F. Merrikh-Bayat, and A. Taheri, "Voltage-mode robust controller design for DC–DC boost converter at the presence of wide load and input voltage variations based on finite-state-machine model," *IET Power Electronics*, vol. 11, no. 5, pp. 866–875, 2018.

[22] A. Ghasemian and A. Taheri, "Constrained near-time-optimal sliding-mode control of boost converters based on switched affine model analysis," *IEEE Transactions on Industrial Electronics*, vol. 65, no. 1, pp. 887–897, 2018.

[23] Q. Chen, S. Xie, M. Sun, and X. He, "Adaptive nonsingular fixed-time attitude stabilization of uncertain spacecraft," *IEEE Transactions on Aerospace and Electronic Systems*, vol. 54, no. 6, pp. 2937–2950, 2018.

[24] M. Tao, Q. Chen, X. He, and M. Sun, "Adaptive nonsingular fixed-time attitude stabilization of uncertain spacecraft," *International Journal of Robust and Nonlinear Control.*vol. 29, no. 12, pp. 4022–4040, 2019.

[25] L. Tao, Q. Chen, and Y. Nan, "Disturbance-observer based adaptive control for second-order nonlinear systems using chattering-free reaching law," *International Journal of Control, Automation and Systems*, vol. 17, no. 2, pp. 356–369, 2019.